

The Art of Modeling and Simulation of Induction Generator in Wind Generation Applications Using High-Order Model

Zhixin Miao^a Lingling Fan^b

^a*Midwest Independent Transmission System Operator, St. Paul MN 55108*

^b*Department of Electrical Engineering, North Dakota State University, Fargo ND 58105*

Abstract

Both fixed-speed squirrel-cage induction generators and variable-speed doubly-fed induction generators are used in wind turbine generation technology. Modeling and simulation of induction machines using vector computing technique in Matlab/Simulink provides an efficient approach for further research on wind generation system integration and control. In this paper, the vector computing technique is applied in modeling and simulation of induction machines. Free acceleration of squirrel-cage induction generator, active power and reactive power control of DFIGs in a power system as well as inter-area oscillation damping control are demonstrated using the proposed model. The modeling approach in Matlab/Simulink makes controller design and simulation verification effective.

Key words: Vector Computing, Induction Generator, DFIG, Oscillation Control, Time Domain Simulation

1 Introduction

Induction machines are important components that serve as power sources and common loads in power systems: pumps, steel mills, servomotors, to name a few. With the increasing use of renewable energy in recent decades, induction generators are found to have important applications in wind turbine generation. Wind turbine driven squirrel-cage induction generators are usually found to interconnect with the grid together with Static Var Compensation (SVC) to

Email addresses: Zhixin.Miao@ieee.org (Zhixin Miao),
Lingling.Fan@ndsu.edu (Lingling Fan).

support reactive power locally [1], [2]. More recently, the doubly-fed induction generator (DFIG) is increasingly used in wind generation. In the case of DFIG, rotor voltages or currents of the induction generators are being controlled. With changing wind speed, one can adjust the frequency of the injected rotor voltage of the DFIG to obtain a constant frequency at the stator [3]. The DFIG is an important type of variable-speed constant-frequency generator. Research on DFIG has shown that it has the ability to control the active power and the reactive power [4] and to provide frequency support [5]. More control applications of DFIG are yet to be investigated. Efficient modeling and simulation techniques for induction generators will facilitate the research on wind turbine generation.

Matlab/Simulink is a powerful tool for time domain simulations. It has been adopted in a graduate level course on modeling and simulation of machines in Purdue University [6]. Yet, in most cases, the featured vector computing technique of Matlab has not been fully explored by electric machine researchers. Using matrix/vector concepts not only simplifies problems but also contributes to time saving in debugging. It makes simulation an art. This concept will be used in dynamic model building and simulation of induction generators in this paper. With modeling task in Simulink accomplished, linearized model can be derived by Matlab with a simple function “linmod”. Linear system analysis and control techniques can be used to develop various control schemes.

Dynamic machinery models are usually expressed by a set of differential equations. In Matlab/Simulink, each differential equation can be represented by an integral unit. With a set of differential equations, a set of integral units will be used. While an input of one integral unit might be a function of the outputs of other integral units, the Simulink model can be very complex and disorganized with lines interweaving. What is more, a less careful design of the model could introduce algebraic loop which will hinder the progress of simulation. Using matrix concepts, a set of differential equations will be expressed as:

$$\dot{X} = AX + BU$$

where X and U are vectors, A and B are matrices. Hence one integral unit is enough to express this model.

The paper will discuss the modeling technique for induction machines. A full order induction generator model building via Matlab/Simulink is investigated in this paper. The model of an induction generator can have various orders, such as 1, 3 or 5. The fifth-order model is considered to be a full order model for an induction generator. The third-order model ignores the stator dynamics and is widely used in power system transient stability analysis [7]. The first-order model ignores both the stator dynamics and the rotor dynamics. The only differential equation left is the swing equation. This model is suitable

for long term power system dynamic study including the induction motor load characteristics [8]. A full order induction generator model includes high bandwidth dynamics and is suitable for current controller design and analysis of its impact on inertial response [9].

Simulations using the full-order dynamic induction generator model will provide researchers insights into the dynamic behavior of the machine, the interaction of the machine and the power electronics control loops. Therefore it is important to develop modeling and simulation based on the full order models of induction generators.

This paper will investigate the vector/matrix form of full order induction generator model and include it into Matlab/Simulink block in Section 2. This block will be tested in various applications, such as free acceleration characteristics of an induction motor, DFIG interconnection with a power system (Section 3), an example power system (Section 4), DFIG current control, active/reactive power control and damping control (Section 5). Simulations are given in Section 6. Section 7 concludes the paper.

2 Induction Machine Model

The voltage equations of an induction machine in an arbitrary reference frame can be written in terms of the currents as shown in Eqn. 1 [10].

$$\begin{bmatrix} v_{qs} \\ v_{ds} \\ v_{0s} \\ v'_{qr} \\ v'_{dr} \\ v'_{0r} \end{bmatrix} = \begin{bmatrix} r_s + \frac{p}{\omega_b} X_{ss} & \frac{\omega}{\omega_b} X_{ss} & 0 & \frac{p}{\omega_b} X_M & \frac{\omega}{\omega_b} X_M & 0 \\ -\frac{\omega}{\omega_b} X_{ss} & r_s + \frac{p}{\omega_b} X_{ss} & 0 & -\frac{\omega}{\omega_b} X_M & \frac{p}{\omega_b} X_M & 0 \\ 0 & 0 & r_s + \frac{p}{\omega_b} X_{ls} & 0 & 0 & 0 \\ -\frac{p}{\omega_b} X_M & \frac{\omega - \omega_r}{\omega_b} X_M & 0 & r'_r + \frac{p}{\omega_b} X'_{rr} & \frac{\omega - \omega_r}{\omega_b} X_M & 0 \\ -\frac{\omega - \omega_r}{\omega_b} X_M & \frac{p}{\omega_b} X_M & 0 & -\frac{\omega - \omega_r}{\omega_b} X'_{rr} & r'_r + \frac{p}{\omega_b} X'_{rr} & 0 \\ 0 & 0 & 0 & 0 & 0 & r'_r + \frac{p}{\omega_b} X'_{lr} \end{bmatrix} \begin{bmatrix} i_{ds} \\ i_{qs} \\ i_{0s} \\ i'_{qr} \\ i'_{dr} \\ i'_{0r} \end{bmatrix} \quad (1)$$

where ω is the rotating speed of the arbitrary reference frame. If we select $\omega = \omega_b$, that is, the rotating speed of the reference frame work is same as $2\pi 60$ rad/s, this reference frame is called a synchronously rotating reference frame or synchronous reference frame.

The air gap flux linkages can be expressed as:

$$\lambda_{qm} = L_M(i_{qs} + i'_{qr}) \quad (2)$$

$$\lambda_{dm} = L_M(i_{ds} + i'_{dr}) \quad (3)$$

and the torque equation can be expressed as:

$$T_e = \lambda_{qm}i_{dr} - \lambda_{dm}i_{qr}. \quad (4)$$

Assume that the reference frame is the synchronous reference frame and that all quantities are in per unit value. Equation (1) can be further written in the form: $\dot{X} = AX + BU$, where $X = [i_{qs}, i_{ds}, i_{os}, i'_{qr}, i'_{dr}, i'_{or}]^T$, and

$$B = \begin{bmatrix} \frac{X_{ss}}{\omega_b} & 0 & 0 & \frac{X_M}{\omega_b} & 0 & 0 \\ 0 & \frac{X_{ss}}{\omega_b} & 0 & 0 & \frac{X_{ss}}{\omega_b} & 0 \\ 0 & 0 & \frac{X_{ls}}{\omega_b} & 0 & 0 & 0 \\ \frac{X_{ss}}{\omega_b} & 0 & 0 & \frac{X'_{rr}}{\omega_b} & 0 & 0 \\ 0 & \frac{X_{ss}}{\omega_b} & 0 & 0 & \frac{X'_{rr}}{\omega_b} & 0 \\ 0 & 0 & 0 & 0 & 0 & \frac{X'_{lr}}{\omega_b} \end{bmatrix}^{-1}; \quad (5)$$

$$A = -B \begin{bmatrix} r_s & \frac{\omega}{\omega_b} X_{ss} & 0 & 0 & \frac{\omega}{\omega_b} X_M & 0 \\ -\frac{\omega}{\omega_b} X_{ss} & r_s & 0 & -\frac{\omega}{\omega_b} X_M & 0 & 0 \\ 0 & 0 & r_s & 0 & 0 & 0 \\ 0 & \frac{\omega - \omega_r}{\omega_b} X_M & 0 & r'_r & \frac{\omega - \omega_r}{\omega_b} X_M & 0 \\ -\frac{\omega - \omega_r}{\omega_b} X_M & 0 & 0 & \frac{\omega - \omega_r}{\omega_b} X'_{rr} & r'_r & 0 \\ 0 & 0 & 0 & 0 & 0 & r'_r \end{bmatrix}. \quad (6)$$

The swing equation is

$$T_e = 2H\dot{\omega}_r + T_m. \quad (7)$$

In summary, the differential equations (Eqn. 1 and Eqn. 7) represent the induction machine with its 5-th order model.

2.1 Induction Machine Simulink Model

The simulink model in terms of the state space equations (Eqn. 1) is shown in Fig. 1. In this model block, the inputs are voltage and rotor speed and the output is a current vector. This model is quite simple and easy to understand.

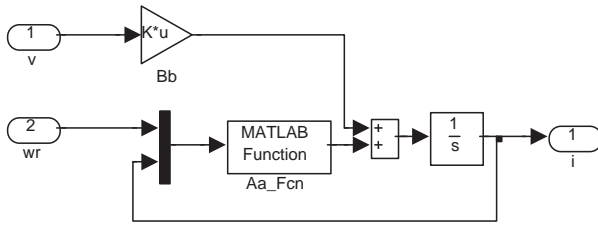


Fig. 1. State Equations in Simulink.

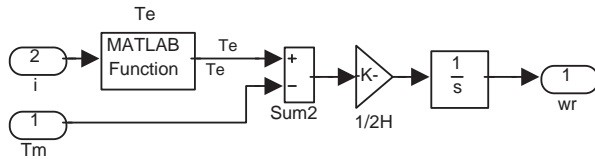


Fig. 2. Swing Equation in Simulink

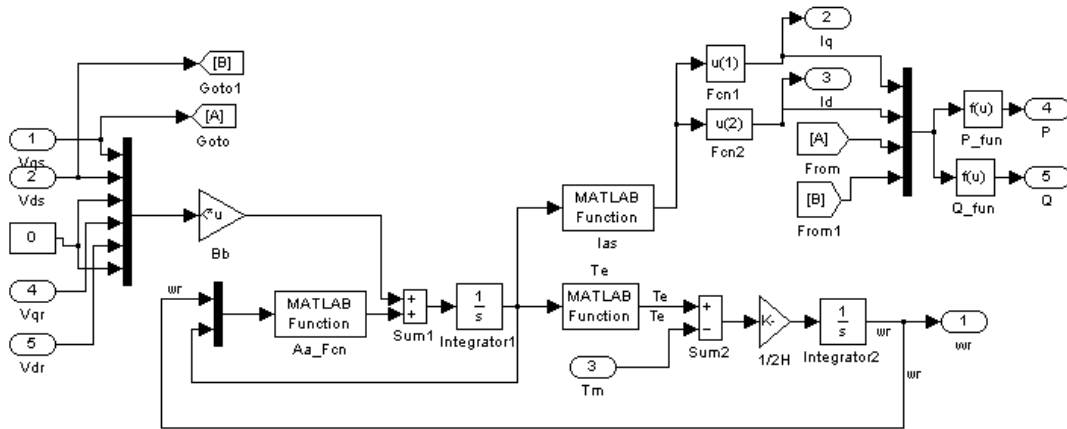


Fig. 3. Induction Generator Modeling in Simulink

It saves not only on model building time but also debugging time. The rotor speed is calculated through Eqn. 7 which is shown in Fig. 2.

The rotor speed will be fed back to the input of the block in Fig. 1. The induction machine serves as a current source to the network and the output from the network is the voltage vector. Thus, the induction machine and the power system network are interconnected and as long as the initial condition is set, dynamic simulation can be performed.

The entire induction generator model block consists both the swing equation and the current state space model. The detailed model in Simulink is shown in Fig. 3.

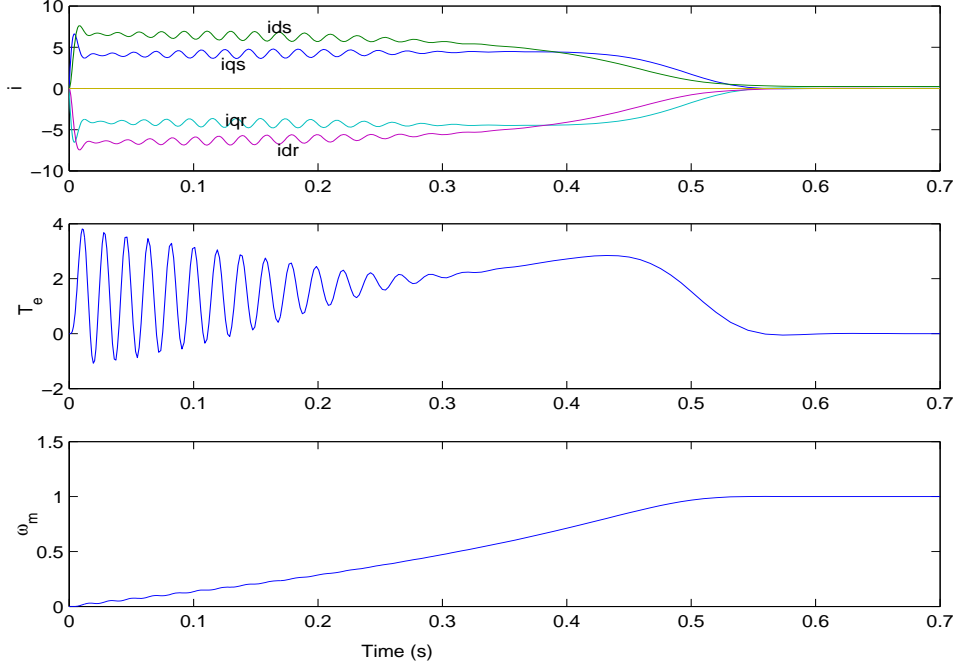


Fig. 4. Free acceleration characteristics of a 10 hp induction motor in the synchronously rotating reference frame

The developed Matlab/Simink model is bench marked by comparing the free acceleration of an induction machine from Krause' book [10]. To simulate the free acceleration, the stator voltages v_{qs} is set to 1 pu and all other voltages v_{ds} , v_{qr} and v_{dr} are set to zero. The rotor is short circuited. The simulation results shown in Fig. 4 are same as those from the textbook.

2.2 DFIG Modeling and Vector Control Concept

In the case of a DFIG, the rotor is not short circuited. A three-phase voltage is injected into the rotor through the converter system. The frequency and magnitude of the output voltage are controlled so that the stator outputs rated voltage at 60 Hz. The DFIG configuration is shown in Fig. 5.

From the voltage equations (Eqn. 1), if we ignore the leakage resistance of the stator, it could be shown that under steady state, v_{ds} is in phase with flux linkage λ_{qm} while v_{qs} is in phase with λ_{dm} . If $v_{ds} = 0$, then $\lambda_{qm} = 0$. Therefore, the alignment of the q-axis with the stator terminal voltage V_s is the same as the alignment of the air gap flux with the d-axis of the reference frame.

The torque equation (4) is now reduced to $T_e = \lambda_{dm}i_{qr}$ and the reactive power Q_s can be expressed in terms of the rotor current as $Q_s = \frac{L_s\lambda_m^2}{L_m^2} - \lambda_m i_{dr}$ [4].

From the expressions for the torque and the reactive power, it is found that

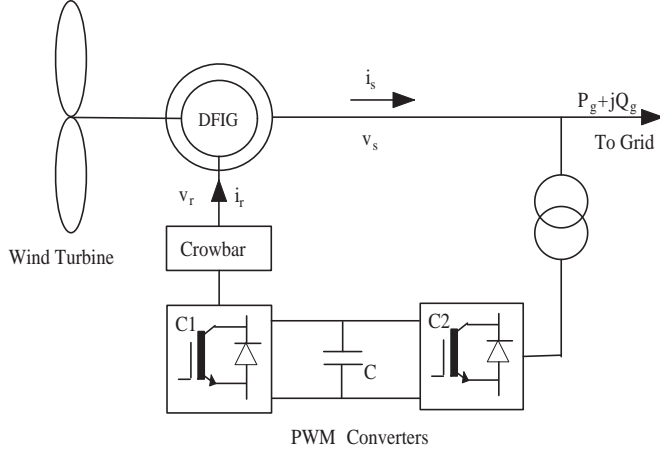


Fig. 5. DFIG configuration

the rotor currents can independently control the real and the reactive power. The rotor currents can in turn be controlled by the injected rotor voltages. The current i_{qr} will be controlled by v_{qr} and i_{dr} will be controlled by v_{dr} . In summary, we can control the active power by controlling v_{qr} and the reactive power by controlling v_{dr} .

3 Interconnection of DFIG Model in Power Systems

Modeling wind farms interconnected to the grid is important for the transient analysis of the entire system. In modeling a power system, the network is usually treated as a Y matrix with the current and voltage relationship as $I = YV$. All generators are treated as current sources. From the current sources, the system voltages can be computed as in Fig. 6. The voltages will then be used in the differential equations expressed in terms of state variables I and input variables V . In the case of a DFIG, the current to the network is the sum of the stator current and the current from the converter and the network voltage is the stator voltage. In a power system, the voltage phasors are all based on a reference bus while the rotor angles are all based on a reference machine. The stator voltage phasor of a DFIG can be expressed as

$$V_s = \frac{v_{qs} - jv_{ds}}{\sqrt{2}} = |V_s| \angle \phi. \quad (8)$$

In this case, the q-axis coincides with the reference voltage direction while the d-axis is lagging the q-axis by 90° .

To facilitate the vector control design for the DFIG, the q-axis has to be aligned with the stator voltage V_s . Therefore, the reference frame of the system

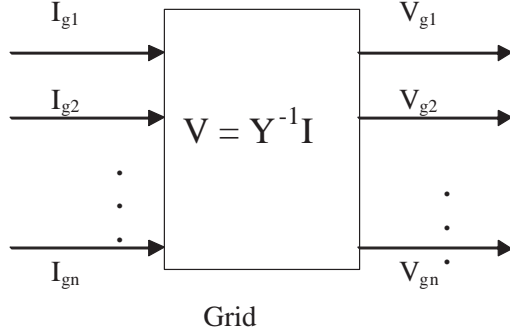


Fig. 6. Grid.

and the reference frame of the DFIG have an angle ϕ between them as in Fig. 7.

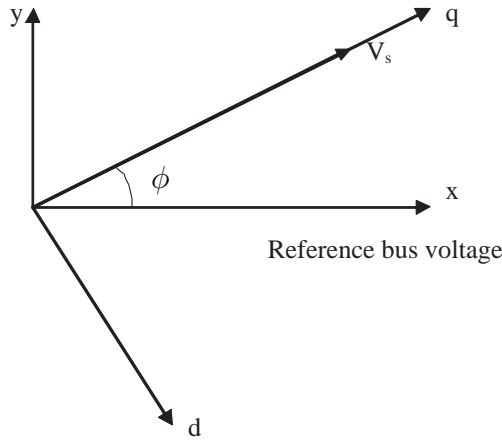


Fig. 7. Machine reference frame and the system reference frame.

If the current to the network is in the machine reference frame, it has to be transformed back to the system reference frame while interconnecting the DFIG to the power system.

The net current injected into the grid consists of the stator current and the current from the converter. If the converter loss is ignored, then the slip power injected to the rotor circuit equals the power flowing from the network to the converter. The PWM converters at grid side have the ability to make the voltage and the current to be in phase. Therefore, the current through the grid side can be computed as $I_a = \frac{P_r}{V_s}$ and the current injected into the grid $I_g = I_s + I_a$, where the rotor injected power is $P_r = (v_{qr}i_{qr} + v_{dr}i_{dr})/\sqrt{2}$. The voltage, current flow diagram is shown in Fig. 8.

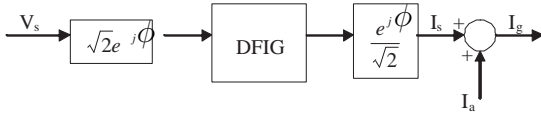


Fig. 8. Interface diagram.

4 An Example Power System

An example power system with a wind farm is presented in this section. The entire model of the system will be built in Matlab/Simulink. The DFIG block and network interface are described in Sections 2 and 3. From this example system, we will show how to use the developed DFIG model to design a damping control scheme.

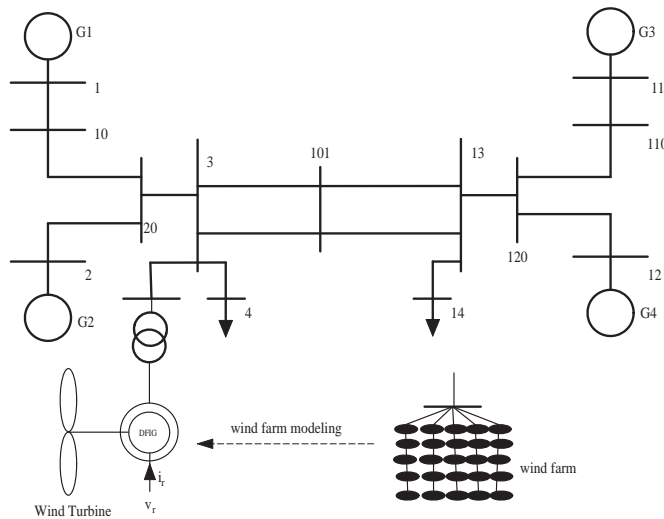


Fig. 9. Line diagram of two-area system with wind generator.

The test system shown in Fig. 9 is based on the classic two-area four-machine system developed in [11] for inter-area oscillation analysis. Area 1 has two synchronous generators, each with 835 MW rated power and Area 2 also has two synchronous generators, each with 835 MW rated power. All four synchronous generators are identical. In Area 1, a wind farm is connected to the grid. Gen 1 exports 700 MW and Gen 2 exports 560 MW. The exporting power level of the wind farm is 240 MW - about 20% of 1260 MW.

In this paper, the full-order model of the synchronous generators is used. The parameters of the steam turbine generators are taken from Krause's classic textbook *Analysis of Electric Machinery* [10]. The parameters are also shown in Appendix.

There exists an inter-area oscillation characterized by the swing of the gen-

erators in Area 1 against the generators in Area 2 and the frequency of the oscillation is about 0.7 Hz or 4.73 rad/s.

With the proposed DFIG model and the network interface technique, we are able to build the entire system described in differential and algebraic equations in Matlab/Simulink. We also assume that the initial slip of the DFIG is -0.1, which means that the DFIG is operating at super synchronous speed.

5 Control of DFIG

The controls of the DFIG include the inner current loop to track a current reference and the outer loop to control the active power and the reactive power. In addition to those controls, in this paper, we also show how to design a supplemental inter-area oscillation damping controller based on the Matlab/Simulink model.

5.1 Inner Current Control Loop of DFIG

The inner current control makes the response of the DFIG faster. Rotor currents are measured and fed back to the controller to generate a suitable rotor voltage. From the voltage equations expressed in (1), the state space model of the currents is already shown in Section 2.

Two PI controllers, one from i_{qr} to v_{qr} and the other from i_{dr} to v_{dr} are used to track the reference rotor current value as in Fig. 10.

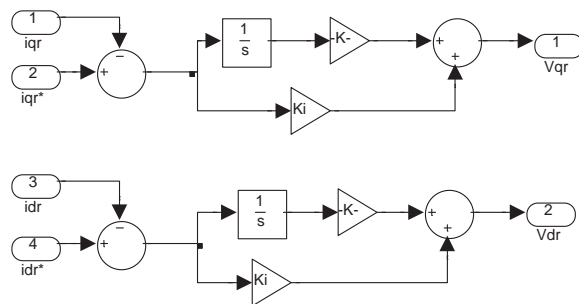


Fig. 10. Current control loops.

The DFIG has a natural oscillation mode of about 60 Hz and hence a higher-than 60 Hz bandwidth means a fast response. The PI controllers are to be designed to have 100 Hz loop gain-crossover-frequency and 90° phase margin

[12]. Using Matlab/Simulink “linmod” function, we can derive the linear state space model from the Simulink model. From the linear state space model, classical control methods can be applied to design the controllers. Bode plots and root loci can all be developed based on the state space model. The parameters of the PI controllers are shown in the Appendix.

5.2 Active Power and Reactive Power Control of DFIG

Active power and reactive power tracking can be achieved by two PI controllers. At steady state, the total generated power should equal to the mechanical power from the wind turbine. The total generated power equals to the difference between the the stator power and the rotor power or $P_g = P_s - P_r$. When the slip is greater than zero or when the wind turbine runs at sub-synchronous speed, $P_r > 0$ or the rotor draws slip power from the grid. When the wind turbine runs at super synchronous speed, $P_r < 0$ or the rotor supplies slip power to the grid. The command of the active power changes when the wind speed changes to extract maximum power from wind [3]. For the test system, the wind speed is assumed to be constant, and hence the power command is assumed to be constant as well.

Power plants are usually required to have the capability to control their reactive power within 0.95 leading to 0.95 lagging range. Therefore, reactive power control is also important in a DFIG system.

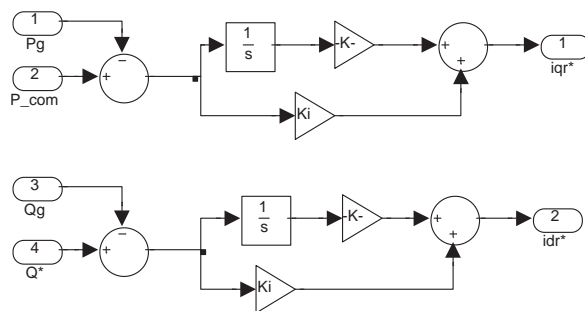


Fig. 11. Active power and reactive power control loops.

The PQ tracking controllers are PI controllers shown in Fig. 11. Due to the decoupling nature of vector control, we can adjust i_{qr} based on P and adjust i_{dr} based on Q .

5.3 Damping Control of DFIG

Since the current loop is very fast and its bandwidth is very high compared to the damping control bandwidth, we will not put a supplementary signal at the current control loop. Instead, we propose to add the supplementary signal at the active power control loop. Since inter-area oscillation is a phenomenon related to the rotor angle and active power, active power modulation is an effective method for oscillation damping in power systems.

The rotor angle difference has a good observability of the inter-area oscillation mode between the two areas [13]. The angle difference signal can be obtained through a state-of-art Phasor Measurement Unit technology. In this paper, we assume that the angle difference signal is available.

The open loop frequency responses of two different systems are compared in Fig. 12. The first system has the input/output pair as P modulation versus the rotor angle difference. The second system has the input/output pair as Q modulation and the rotor angle difference.

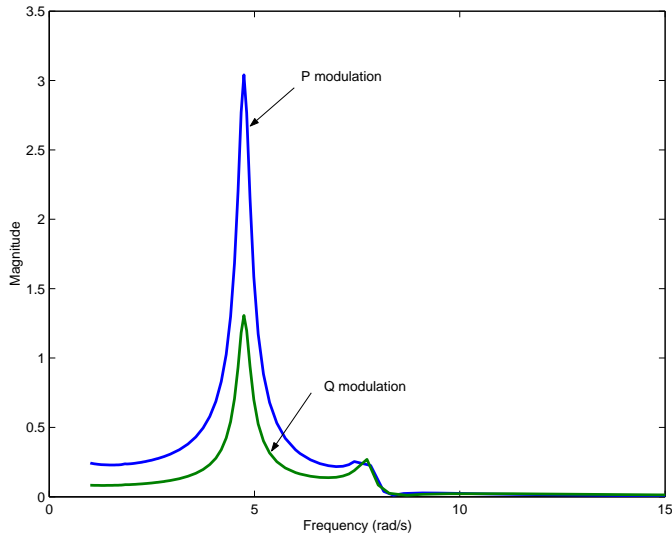


Fig. 12. Open-loop frequency responses with P modulation or Q modulation

It is seen that at the oscillation frequency is about 4 rad/s and the first system has a higher magnitude compared to the second system. To control the first system, we will need a smaller gain. Smaller gain is preferred since it avoids controller saturation. The frequency responses confirm that active power modulation is a good choice for inter-area oscillation damping. Therefore, we use P modulation for inter-area oscillation damping control.

The overall control structure of the DFIG rotor side converter is shown in Fig. 13. The damping control scheme is shown in Fig. 14.

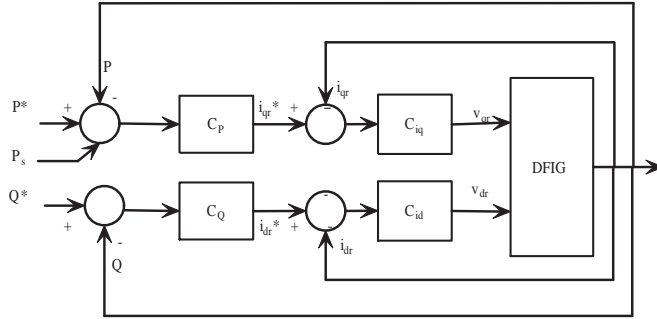


Fig. 13. The overall control structure of the DFIG rotor side converter

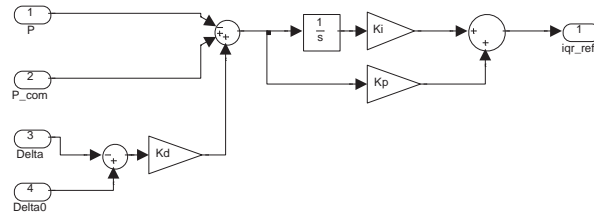


Fig. 14. Damping control scheme.

The root locus diagram of the open loop system is shown in Fig. 15. The open loop system is unstable since there are two pairs of complex poles on the right half plane. One pair of poles correspond to the inter-area oscillation mode at 4.73 rad/s and the other pair corresponds to an oscillation mode at 7.74 rad/s. The second pair of poles have the associated zeros close by and hence it is difficult to move the second pair of poles to the left half plan. The best option is to move the poles close to the zeros as fast as possible with gain increasing.

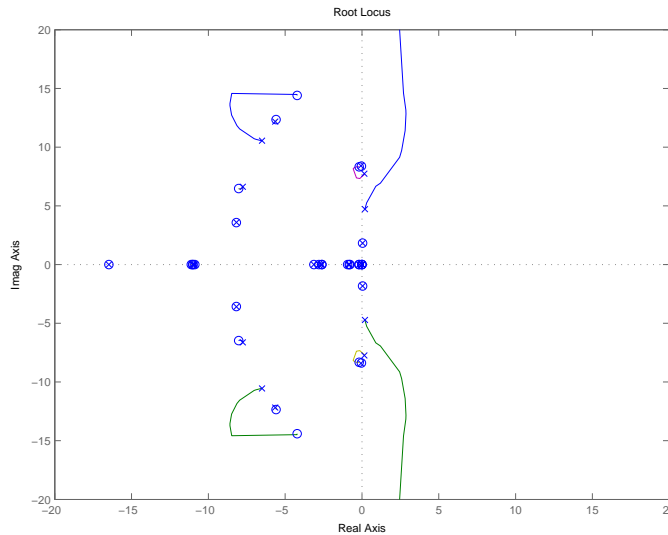


Fig. 15. Root locus of the open loop

A proportional controller cannot do the job. This is due to the fact that the two oscillation modes (root locus) will move in opposite directions according to the root locus diagram. Moving one mode to the left plane means moving the other mode to the right plane. Thus a more complicated controller is required. The open-loop system has a high order and the design is simplified by considering the dominant zeros and poles only. The transfer function of the simplified system is shown as:

$$P = -\frac{(s + 0.1 \pm j8.43)(s + 4.22 \pm j14.5)}{(s - 0.209 \pm j4.79)(s - 0.25 \pm j7.9)(s + 6.5 \pm j10.5)}. \quad (9)$$

The frequency response of the simplified system P is compared with the original open loop system (Fig. 16). It is found that the phase angles over the frequency range 1-100 rad/s are the same. However, there are differences in the magnitudes. Providing P with a gain $k = 3$ makes Pk have the same frequency response as the original open-loop system as shown in Fig. 16.

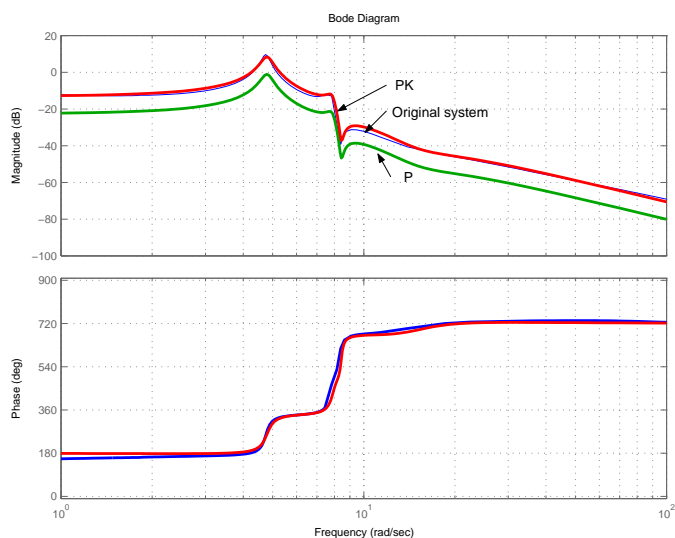


Fig. 16. Bode plots of the system and the simplified system

We now use the modified low-order system Pk to design a controller that can move the two pairs of unstable poles to the left plane. It is found that the first pair of poles corresponds to the inter-area oscillation mode. The frequency of the mode in the open-loop system is 4.73 rad/s. The second pair of the poles corresponds to a oscillation mode with a frequency of 7.74 rad/s. Apparently, the selected input signal (rotor angle difference) is not effective in enhancing the damping of the second oscillation mode since the poles are very close to the zeros. To enhance the damping of the inter-area oscillation mode, a pair of complex zeros are added in the left plane close to the poles to attract the poles to the left plane when the gain increases. To make the controller proper, two real poles on the left real axis are also added. To make the second pair of poles

move to the corresponding zeros as fast as possible, two pairs of zeros-poles nearby are added.

The transfer function of the controller G_d is given by

$$G_d = \frac{(1 + 0.052s + 0.332s^2)(1 + 0.0084s + 0.162s^2)}{(1 + 0.12s)(1 + 0.049s)(1 + 0.0063s + 0.0892s^2)}. \quad (10)$$

The root locus diagram of the compensated system G_dP is shown in Fig. 17.

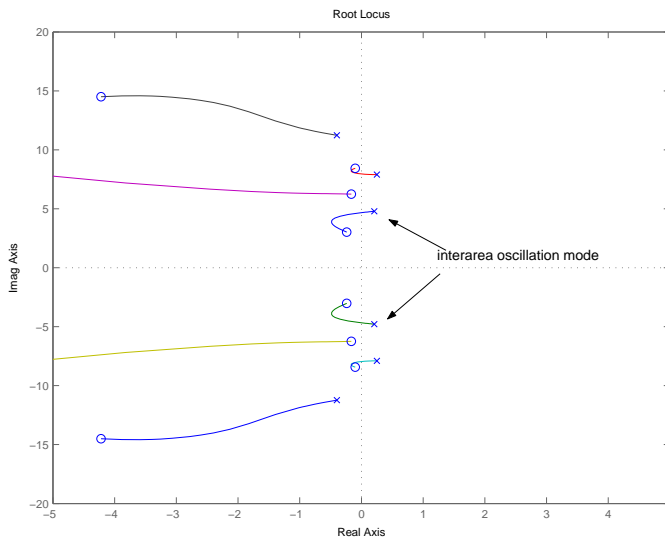


Fig. 17. Root locus after compensation

The gain that corresponds to maximum damping ratio for the inter-area oscillation mode is picked from the root locus diagram. Here the gain is chosen as 5 and the final damping controller designed is given by $K_d = 5G_d$.

6 Simulation Results

Time-domain simulation is performed on the test system. The system will operate under steady state for 0.1 second. The power transfer between the two areas is 400 MW. A temporary three-phase fault occurs at Bus 3 and is cleared after 0.1 second. Figs. 18 and 19 show the dynamic responses of the synchronous generators and the DFIG when there is no inter-area oscillation control. In Fig. 18, the relative angle differences, rotor speeds and electric power exporting levels are plotted. In Fig. 19, the DFIG rotor speed, DFIG mechanical torque, electric torque and terminal voltage are plotted. The system suffers from low-frequency oscillations and as time goes by, the oscillations increase and the system becomes unstable.

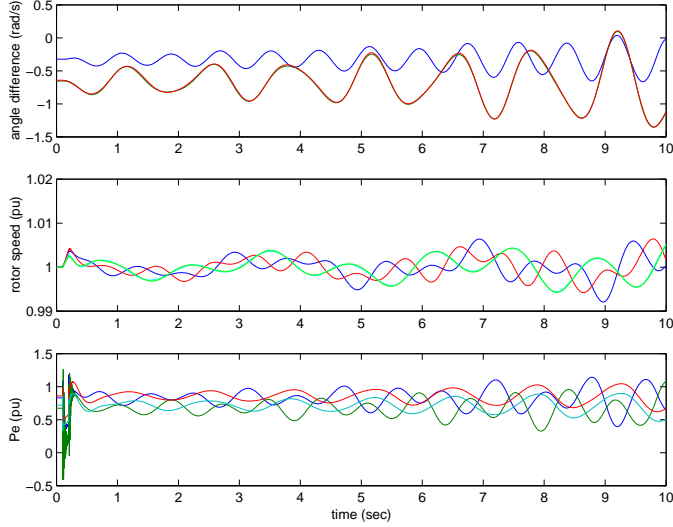


Fig. 18. Synchronous generator dynamic responses with no supplementary damping control. (a) Relative rotor angles δ_{21} , δ_{31} and δ_{41} . (b) Rotor speeds of the four synchronous generators. (c) Output power levels from the four synchronous generators.

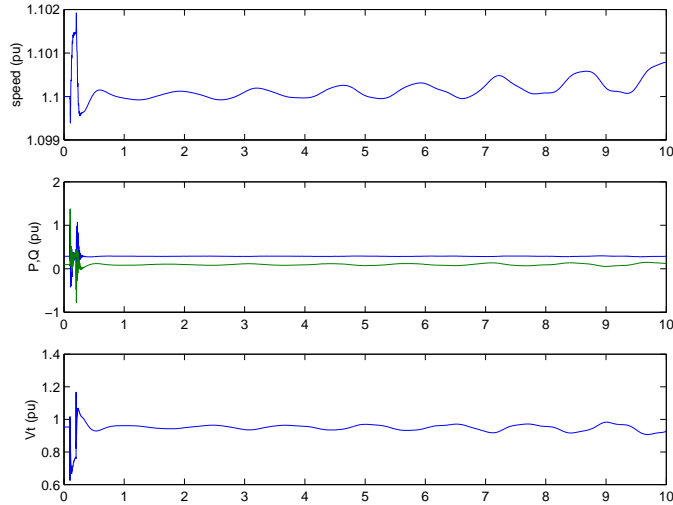


Fig. 19. Wind turbine generation dynamic responses with no supplementary damping control. (a) Speed of DFIG rotor. (b) Output P and Q of the DFIG (P is above curve Q). (c) Terminal voltage magnitude of the DFIG.

Figs. 20-22 show the dynamic responses of the synchronous generators, the induction generator, damping controller input/output and DFIG rotor voltage v_{qr} and v_{dr} with the auxiliary damping control added for active power modulation.

The dynamic responses of the rotor angles are plotted together for the two scenarios: 1) with no damping control, and 2) with damping control. The plots are shown in Fig. 23 where the dashed lines correspond to the first scenario and the solid lines correspond to the second scenario. From the plots, we can verify the effectiveness of the damping controller to damp out the 0.7 Hz inter-area

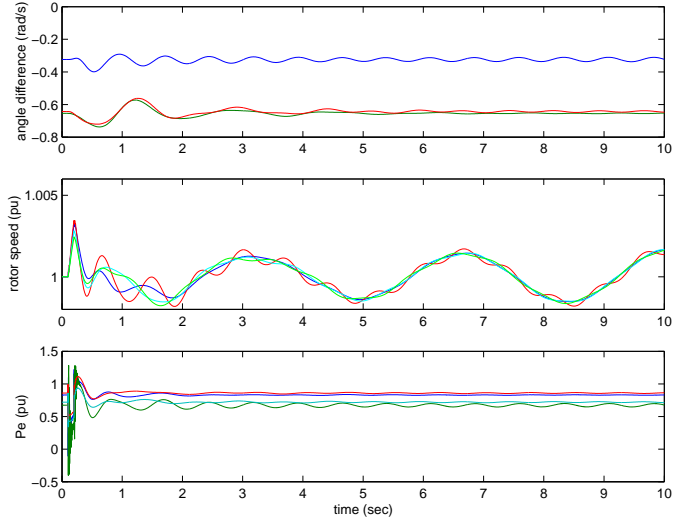


Fig. 20. Synchronous generator dynamic responses with supplementary damping control. (a) Relative rotor angles δ_{21} , δ_{31} and δ_{41} . (b) Rotor speeds of the four synchronous generators. (c) Output power levels from the four synchronous generators.

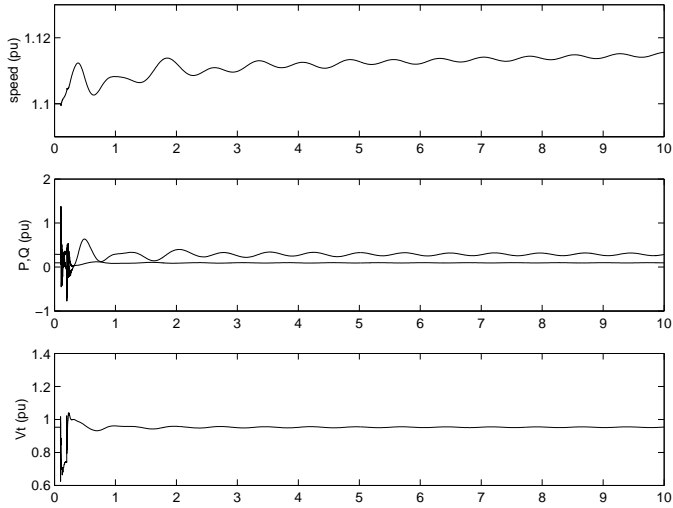


Fig. 21. Wind turbine generator dynamic responses with supplementary damping control. T (a) Speed of DFIG rotor. (b) Output P and Q of the DFIG (P is above curve Q). (c) Terminal voltage magnitude of the DFIG.

oscillation. Meanwhile the other oscillation mode tends to damp out as well. Compared to the originally unstable case, the modified system becomes stable with the addition of a supplementary control loop. The enhanced stability can further help to improve the transfer capability and move more wind power to the market.

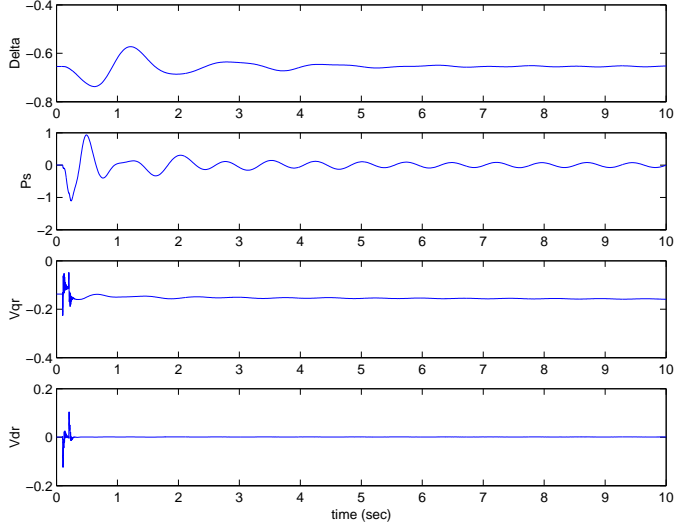


Fig. 22. Damping control input, output signals and v_{qr} and v_{dr} dynamic responses.

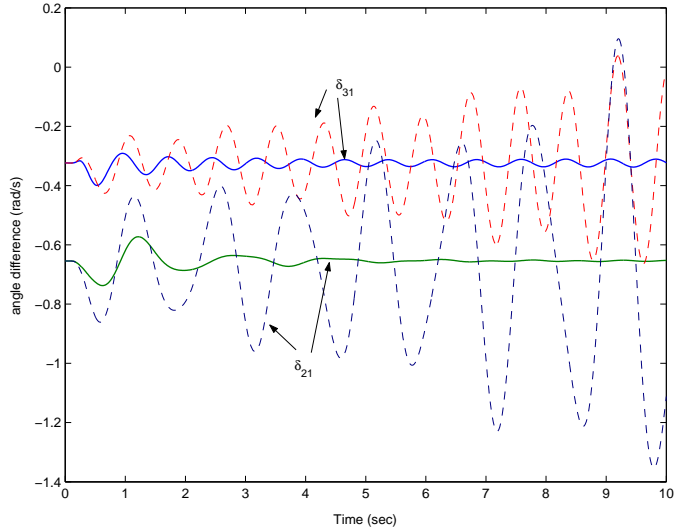


Fig. 23. Comparison of rotor angle dynamic responses.

7 Conclusion

This paper proposes a methodology to model induction machines in Matlab/Simulink using matrix/vector concept. This methodology greatly saves the modeling time and debugging time. Models built in this way are easy to be understood by students and engineers. The integration of the developed DFIG model with the network is presented in the paper. The interconnecting technique takes into consideration the DFIG vector control scheme by transferring voltage and current phasors between two reference frames. The design of the DFIG rotor-side converter control is also demonstrated in this paper. The effectiveness of the inner current control loops, the active and reactive control loops as well as the inter-area oscillation damping control loops is also

demonstrated through simulation.

8 Acknowledgement

The authors would like to thank Dr. Subbaraya Yuvarajan and anonymous reviewers for reviewing the manuscript. This work is sponsored in part by NSF EPSCoR through Grant EPS-0447679.

Appendix

Synchronous generator parameters:

Rating: 835 MVA, line to line voltage: 26 kV, poles: 2, speed: 3600 r/min

Combined inertia of generator and turbine: $H = 5.6$ s

$r_s = 0.00243\Omega$, 0.003 pu, $X_{ls} = 0.1538\Omega$, 0.19 pu

$X_q = 1.457\Omega$, 1.8pu, $X_d = 1.457\Omega$, 1.8pu

$r'_{kq1} = 0.00144\Omega$, 0.00178pu, $r'_{fd} = 0.00075\Omega$, 0.000929pu

$X'_{lkq1} = 0.6578\Omega$, 0.8125pu, $X'_{lfd} = 0.1165\Omega$, 0.1414pu

$r'_{kq2} = 0.00681\Omega$, 0.00841pu, $r'_{kd} = 0.01080\Omega$, 0.01334pu

$X'_{lkq2} = 0.07602\Omega$, 0.0939pu, $X'_{lkd} = 0.06577\Omega$, 0.08125pu

Induction generator parameters:

$H = 5$ s, $r_s = 0.00059$ pu, $X_M = 0.4161$ pu, $r_r = 0.00339$ pu, $X_{ls} = 0.0135$ pu,

$X_{lr} = 0.0075$ pu.

Current control loops: $0.0352 + \frac{1.6765}{s}$.

PQ control loops: $1 + \frac{1}{s}$.

References

- [1] Z. Miao, Modeling and dynamic stability of distributed generations, Ph.D. thesis, West Virginia University (2002).
- [2] E. Abdin, W. Xu, Control design and dynamic performance analysis of a wind turbine induction generator unit, IEEE Trans. Energy Conversion 15 (1) (2000) 91–96.
- [3] S. Muller, M. Deicke, R. W. D. Doncker, Doubly fed induction generator systems for wind turbine, IEEE Ind. Appl. Mag. (2002) 26–33.

- [4] L. Xu, W. Cheng, Torque and reactive power control of a doubly fed induction machine by position sensorless scheme, *IEEE Trans. Ind. Applicat.* 31 (3) (1995) 636–642.
- [5] J. Ekanayake, N. Jenkins, Comparison of response of doubly fed and fixed-speed induction generator wind turbines to changes in network frequency, *IEEE Trans. Energy Conversion* 19 (2004) 800–802.
- [6] C.-M. Ong, *Dynamic Simulation of Electric Machinery using Matlab/Simulink*, Prentice Hall PTR, Upper Saddle River, New Jersey 07458, 1998.
- [7] Y. Lei, A. Mullane, G. Lightbody, R. Yacamini, Modeling of the wind turbine with a doubly fed induction generator for grid integration studies, *IEEE Trans. Energy Conversion* 21 (2006) 257–264.
- [8] D. Popovic, I. Hiskens, D. Hill, Stability analysis of induction motor networks, *International Journal of Electrical Power and Energy Systems* 20 (7) (1998) 475–487.
- [9] A. Mullane, M. O'Malley, The inertial response of induction-machine-based wind turbines, *IEEE Trans. Power Syst.* 20 (3) (2005) 1496–1503.
- [10] P. C. Krause, O. Wasynczuk, S. D. Sudhoff, *Analysis of Electric Machinery*, IEEE Press, Piscataway, NJ 08855, 1995.
- [11] M. Klein, G. Rogers, P. Kundur, A fundamental study of inter-area oscillations in power systems, *IEEE Trans. Power Syst.* 6 (1991) 914–921.
- [12] T. K. A. Brekken, N. Mohan, Control of a doubly fed induction wind generator under unbalanced grid voltage conditions, *IEEE Trans. Energy Conversion* 22 (1) (2007) 129–135.
- [13] E. Larsen, J. J. Sanchez-Gasca, J. Chow, Concepts for design of FACTS controllers to damp power swings, *IEEE Trans. Power Syst.* 10 (1995) 948–956.